

# Learned Scalable Video Coding For Humans and Machines

Hadi Hadizadeh and Ivan V. Bajić, *Senior Member, IEEE*

**Abstract**—Video coding has traditionally been developed to support services such as video streaming, videoconferencing, digital TV, and so on. The main intent was to enable human viewing of the encoded content. However, with the advances in deep neural networks (DNNs), encoded video is increasingly being used for automatic video analytics performed by machines. In applications such as automatic traffic monitoring, analytics such as vehicle detection, tracking and counting, would run continuously, while human viewing could be required occasionally to review potential incidents. To support such applications, a new paradigm for video coding is needed that will facilitate efficient representation and compression of video for both machine and human use in a scalable manner. In this manuscript, we introduce the first end-to-end learnable video codec that supports a machine vision task in its base layer, while its enhancement layer supports input reconstruction for human viewing. The proposed system is constructed based on the concept of conditional coding to achieve better compression gains. Comprehensive experimental evaluations conducted on four standard video datasets demonstrate that our framework outperforms both state-of-the-art learned and conventional video codecs in its base layer, while maintaining comparable performance on the human vision task in its enhancement layer. We will provide the implementation of the proposed system at [www.github.com](http://www.github.com) upon completion of the review process.

**Index Terms**—video compression, video analytics, scalable coding, deep learning, coding for machines

## I. INTRODUCTION

VIDEO analytics is a crucial technology that finds application in a wide range of fields, such as visual surveillance, traffic monitoring, and autonomous navigation. In many applications, input video is compressed and transmitted to the cloud for subsequent analysis. Depending on the specific application, two primary approaches can be adopted. When machine-based video analytics is the sole focus, precomputed features can be compressed and transmitted to the cloud instead of the complete video, thus reducing the required bandwidth [1]. Various hand-crafted and neural-network-based (learned) approaches have been developed to serve this purpose [2], [3]. However, if human viewing is also required, the input video must also be encoded and transmitted, increasing the complexity of the system.

The other alternative approach involves compressing the input video in a conventional way and transmitting it to the cloud, where it will be decoded and used for visual analysis. Various standard and non-standard video codecs have been proposed over the last few decades for this purpose, including

High Efficiency Video Coding (HEVC) [4] and Versatile Video Coding (VVC) [5]. However, if human viewing is needed only occasionally, this approach is inefficient, as will be shown later in the paper.

The swift progress in deep learning technologies has led to the emergence of several learned image and video codecs that rely on deep neural networks (DNNs) to compete with established conventional counterparts like JPEG, HEVC, and VVC. Notable methods include [6], [7], [8], [9], [10], [11], [12], [13], [14]. Nevertheless, a majority of DNN-based codecs have focused on image and video compression for human viewing. On the other hand, DNNs are widely used in visual analytics, but their primary emphasis is not on compression [15].

Recently, a new standardization effort, known as MPEG-VCM (Video Coding for Machines) [16], has been initiated with the aim of establishing a standardized framework for video coding that caters to the needs of both human and machine vision. Various approaches have also been proposed for scalable image coding for multiple tasks [17], [18], [19], including machine vision and human viewing. In these methods, the base layer usually supports the machine vision task (e.g., object detection) while the enhancement layer supports input reconstruction for human viewing. In terms of video, [20] presents a scalable human-machine video codec based on the concept of latent-space scalability [21]. This codec was designed using a hybrid approach that leverages DNN-based compression for intra coding, and a combination of DNN and conventional techniques inter-frame coding.

As discussed in [19], a typical machine vision pipeline involves image encoding, decoding, and the analysis of the decoded image by a machine vision model. This process can be represented by a Markov chain [22]  $X \rightarrow Y \rightarrow \hat{X} \rightarrow V$ , where  $X$  denotes the input image,  $Y$  represents the latent representation of  $X$ ,  $\hat{X}$  is the reconstructed image, and  $V$  is the output of the machine vision model. Applying the data processing inequality [22] to this chain, we can infer that  $I(Y; \hat{X}) \geq I(Y; V)$ , where  $I(\cdot; \cdot)$  represents the mutual information [22]. This suggests that machine vision requires less information (fewer bits) than input reconstruction. This aligns with scalable human-machine coding approaches mentioned above, where both base and enhancement layers are utilized for input reconstruction, but only the base layer (i.e., fewer bits) is used for machine vision.

In this paper, we present the first (to our knowledge) end-to-end learned scalable human-machine video codec. The proposed codec is designed to support object detection in its base layer, and input reconstruction by using both base and enhancement layer. The proposed system utilizes the back-

H. Hadizadeh and I. V. Bajić are with the School of Engineering Science, Simon Fraser University, Burnaby, BC, V5A 1S6, Canada, e-mail: [ibajic@ensc.sfu.ca](mailto:ibajic@ensc.sfu.ca).

end of a well-known DNN-based object detection network (YOLOv5) [23] to execute the object detection task through its base layer. However, the architecture of the proposed system is versatile, and it can be seamlessly integrated with other machine vision models. In terms of compression, the proposed system is constructed based on the notion of conditional coding [9], [10], [14], [24], which is theoretically more efficient than the widely-employed residual coding.

The proposed system differs from [20] in several ways. First, [20] is a hybrid codec that incorporates both DNN-based and conventional handcrafted video coding tools, while the system presented in this paper is an end-to-end learned codec. Second, [20] used only intra-coding in the base layer, while our proposed system utilizes inter-frame coding for both the base and enhancement layers. Third, [20] employed conventional residual inter-frame coding in the enhancement layer, while our proposed codec is built upon conditional coding, which is theoretically more efficient. Finally, [20] used YOLOv3 [25] for object detection in the base layer while our codec uses the more recent YOLOv5 [23].

Our experiments on four standard video datasets demonstrate that the base layer of the proposed system outperforms state-of-the-art conventional and learned video codecs in coding for object detection, while the enhancement layer provides comparable performance for human viewing to those obtained by the existing codecs. The proposed codec is well suited for applications where automated machine vision needs to run continuously while human viewing is needed occasionally, which we demonstrate through break-even analysis.

This paper is organized as follows. We first provide our motivation for using the concept of conditional coding for our codec design in Section II. The proposed system is presented in Section III. The experimental results are provided in Section IV, and the conclusions are drawn in Section V.

## II. MOTIVATION

In this section we provide motivation for our compression approach by analyzing residual and conditional coding from the rate-distortion point of view. We will use capital letters ( $X$ ) to denote random variables and lowercase letters ( $x$ ) for their realizations.

Conditional coding has been argued in [9], [10], [12], [14], [24] to offer the potential for better compression performance compared to residual coding. However, these studies offered only arguments based on lossless compression. Specifically, if  $X$  is the input to be compressed and  $Y$  is its predictor, then it can be shown [24] that

$$H(X|Y) \leq H(X - Y), \quad (1)$$

where  $H(\cdot)$  is the entropy and  $H(\cdot|\cdot)$  is the conditional entropy [22]. If we were interested in lossless coding, this would be enough to motivate the choice of a conditional codec over a residual one, since entropy is the limit of lossless compression. However, most practical codecs are lossy, so we need to employ rate-distortion theory to argue in favor of conditional versus residual coding. In this section, we offer such analysis, which can be considered as the extension of (1) into the realm of rate-distortion.

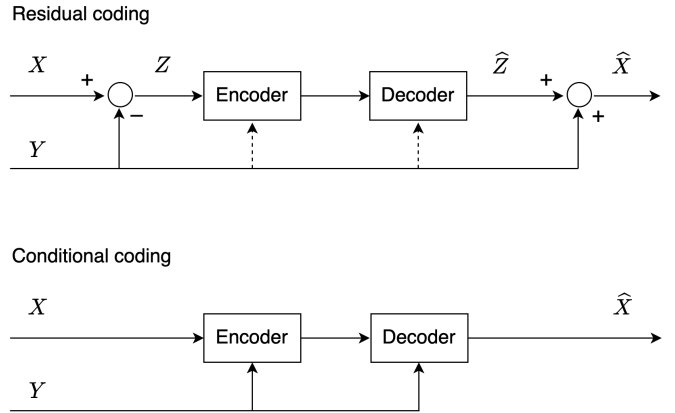


Fig. 1. Top: residual coding. Dashed lines are not used in residual coding, they are shown to aid the analysis in the text. Bottom: conditional coding.

First we need to recall a few concepts from rate-distortion theory [22]. Let  $d(x, \hat{x})$  be a distortion measure between an input  $x$  and its reconstruction  $\hat{x}$ . The expected distortion between input  $X$  and its reconstruction  $\hat{X}$  is computed as

$$\mathbb{E} [d(X, \hat{X})] = \sum_{x, \hat{x}} p_X(x) \cdot p_{\hat{X}|X}(\hat{x}|x) \cdot d(x, \hat{x}), \quad (2)$$

where  $p_X(x)$  is the input distribution and  $p_{\hat{X}|X}(\hat{x}|x)$  is the conditional distribution of the reconstruction given the input, also known as the *quantizer*. The input distribution is not under our control, but the quantizer is. For a given distortion level  $D > 0$ , the set of feasible quantizers for  $X$  that achieve expected distortion of at most  $D$  is denoted

$$\mathcal{P}_X(D) = \left\{ p_{\hat{X}|X}(\hat{x}|x) : \mathbb{E} [d(X, \hat{X})] \leq D \right\}. \quad (3)$$

The rate distortion function  $R(D)$  is the minimum achievable rate for encoding input  $X$  while incurring expected distortion of at most  $D$ . It is given by:

$$R(D) = \min_{p_{\hat{X}|X}(\hat{x}|x) \in \mathcal{P}_X(D)} I(X; \hat{X}), \quad (4)$$

where  $I(\cdot; \cdot)$  is the mutual information [22]. Note that in rate-distortion theory, rate is governed by mutual information rather than entropy, which is why (1) cannot be used directly to motivate conditional lossy compression.

Consider the two coding schemes illustrated in Fig. 1, where the top part shows residual coding and the bottom part shows conditional coding. In residual coding, prediction  $Y$  is subtracted from the input  $X$  to create  $Z = X - Y$ , which is then encoded and reconstructed as  $\hat{Z}$ . Finally, input reconstruction is obtained as  $\hat{X} = \hat{Z} + Y$ . If the distortion is shift-invariant<sup>1</sup> then  $d(x, \hat{x}) = d(x - y, \hat{x} - y) = d(z, \hat{z})$ , so  $\mathbb{E}[d(X, \hat{X})] = \mathbb{E}[d(Z, \hat{Z})]$ . Hence, the rate-distortion function for residual coding of  $X$  is

$$R_r(D) = \min_{p_{\hat{Z}|Z}(\hat{z}|z) \in \mathcal{P}_Z(D)} I(Z; \hat{Z}), \quad (5)$$

<sup>1</sup>Many conventional distortion measures, including norm-based measures, are shift-invariant.

where subscript  $r$  indicates residual coding and

$$\mathcal{P}_Z(D) = \left\{ p_{\hat{z}|Z}(\hat{z}|z) : \mathbb{E} \left[ d(X, \hat{X}) \right] \leq D \right\}. \quad (6)$$

Meanwhile, the rate-distortion function for conditional coding of  $X$  relative to  $Y$  (Fig. 1 bottom) is

$$R_c(D) = \min_{p_{\hat{X}|X,Y}(\hat{x}|x,y) \in \mathcal{P}_{X|Y}(D)} I(X; \hat{X}|Y), \quad (7)$$

where subscript  $c$  indicates conditional coding,  $I(\cdot; \cdot|Y)$  is the conditional mutual information [22], and

$$\mathcal{P}_{X|Y}(D) = \left\{ p_{\hat{X}|X,Y}(\hat{x}|x,y) : \mathbb{E} \left[ d(X, \hat{X}) \right] \leq D \right\}. \quad (8)$$

We expand  $I(X; \hat{X}|Y)$  as follows:

$$\begin{aligned} I(X; \hat{X}|Y) &= H(X|Y) - H(X|\hat{X}, Y) \\ &\stackrel{(a)}{=} H(X - Y|Y) - H(X - Y|\hat{X}, Y) \\ &= I(X - Y; \hat{X}|Y) \\ &= H(\hat{X}|Y) - H(\hat{X}|Y, X - Y) \\ &\stackrel{(b)}{=} H(\hat{X} - Y|Y) - H(\hat{X} - Y|Y, X - Y) \\ &= I(X - Y; \hat{X} - Y|Y) \\ &\stackrel{(c)}{=} I(Z; \hat{Z}|Y), \end{aligned} \quad (9)$$

where (a) (resp. (b)) follows from the fact that given  $Y$ , the only uncertainty in  $X - Y$  (resp.  $\hat{X} - Y$ ) is due to  $X$  (resp.  $\hat{X}$ ), and (c) follows from the fact that  $Z = X - Y$  and  $\hat{Z} = \hat{X} - Y$ . Moreover, due to these relationships, it should be clear that conditioned on  $Y$ , minimization over  $p_{\hat{X}|X,Y}(\hat{x}|x,y)$  is equivalent to minimization over  $p_{\hat{Z}|Z,Y}(\hat{z}|z,y)$ . Combining this with (9), we have that  $R_c(D)$  from (7) can also be written as

$$R_c(D) = \min_{p_{\hat{Z}|Z,Y}(\hat{z}|z,y) \in \mathcal{P}_{Z|Y}(D)} I(Z; \hat{Z}|Y), \quad (10)$$

where

$$\mathcal{P}_{Z|Y}(D) = \left\{ p_{\hat{Z}|Z,Y}(\hat{z}|z,y) : \mathbb{E} \left[ d(X, \hat{X}) \right] \leq D \right\}. \quad (11)$$

Hence, conditional coding of  $X$  relative to  $Y$  achieves the same rate distortion as conditional coding of  $Z$  relative to  $Y$ . This is shown in Fig. 1(top), where the dashed line indicates conditional coding, mimicking Fig. 1(bottom).

Next, we note that  $\mathcal{P}_Z(D) \subset \mathcal{P}_{Z|Y}(D)$ , because the set  $\mathcal{P}_{Z|Y}(D)$  includes distributions in which  $\hat{Z}$  is conditionally (given  $Z$ ) independent of  $Y$ . Hence, minimizing  $I(Z; \hat{Z}|Y)$  over  $\mathcal{P}_{Z|Y}(D)$  cannot be any worse than minimizing  $I(Z; \hat{Z})$  over  $\mathcal{P}_Z(D)$ . For this reason,

$$R_c(D) \leq R_r(D), \quad (12)$$

meaning that for any given distortion level  $D > 0$ , (optimal) conditional coding achieves the rate no higher than (optimal) residual coding. Equation (12) is the rate-distortion analog of (1). In fact, (1) provides the result for the special case  $D = 0$  (lossless coding), while (12) extends this to  $D > 0$ . Intuition behind it is shown in Fig. 1(top), where the dashed lines imply that the conditional codec for  $Z$  can, at the very least, ignore  $Y$ , and thereby match any performance that residual codec can achieve.

### III. PROPOSED METHOD

In this section, we present our proposed scalable video coding system, which is composed of a base layer and an enhancement layer. We first present the problem statement in Section III-A. We then describe the structure of the base layer in Section III-B, followed by the structure of the enhancement layer in Section III-C. The overall block diagram of the proposed system is depicted in Fig. 2.

#### A. Problem Statement

Let  $x_{1:T} \in \mathbb{R}^{T \times 3 \times H \times W}$  denote a raw (RGB) video sequence of  $T$  frames  $\{x_t, t = 1, \dots, T\}$  each of width  $W$  and height  $H$ . The aim is to design an end-to-end learnable system to code the input video in a scalable manner that caters to both machine vision and human viewing. We design a system whose base layer facilitates object detection, intended for machine usage, while the enhancement layer, together with the base layer, facilitates reconstruction of the input video for human viewing. In our design, we exploit the concept of conditional coding which, as shown in the previous section, holds theoretical advantage over the more common residual coding.

The base layer encoder codes every video frame,  $x_t$ , into a compressed base layer bitstream. The base layer decoder then decodes the compressed bitstream to obtain a decoded RGB frame,  $\hat{x}_t^b$ , also referred to as the decoded *base frame*. This frame is utilized by a computer vision (CV) model (in our case YOLOv5 [23]) for video analysis (in our case object detection). Furthermore,  $\hat{x}_t^b$  also helps the enhancement layer perform the reconstruction of the input frame for human viewing. The base layer is trained to maximize object detection accuracy while minimizing the rate of the base layer's bitstream.

The input video frame,  $x_t$ , is also fed into the enhancement layer alongside the decoded base frame,  $\hat{x}_t^b$ . The enhancement layer's encoder then compresses the input frame conditionally to generate a compressed bitstream, which the enhancement layer's decoder utilizes to reconstruct an output frame,  $\hat{x}_t$ . The enhancement layer is trained end-to-end to minimize both the distortion between  $x_t$  and  $\hat{x}_t$ , as well as the rate of the enhancement layer's bitstream. In the proposed system, the base layer is trained first, followed by training the enhancement layer while keeping the base layer frozen. In scalable human-machine image coding, this strategy has recently been shown to be advantageous over parallel training of the base and enhancement layer [26], so we use it for our proposed video codec as well.

It is important to note that in practice, if the sole objective is to perform the computer vision task, there is no need to reconstruct the input frame. That is, the enhancement layer's bitstream does not need to be created because  $\hat{x}_t$  does not need to be reconstructed at the decoder. If human viewing is required, the enhancement layer can be employed and  $\hat{x}_t$  reconstructed. Many video analytics applications, such as traffic monitoring or video surveillance, require continuous use of the analytics engine (base layer in our system), and only

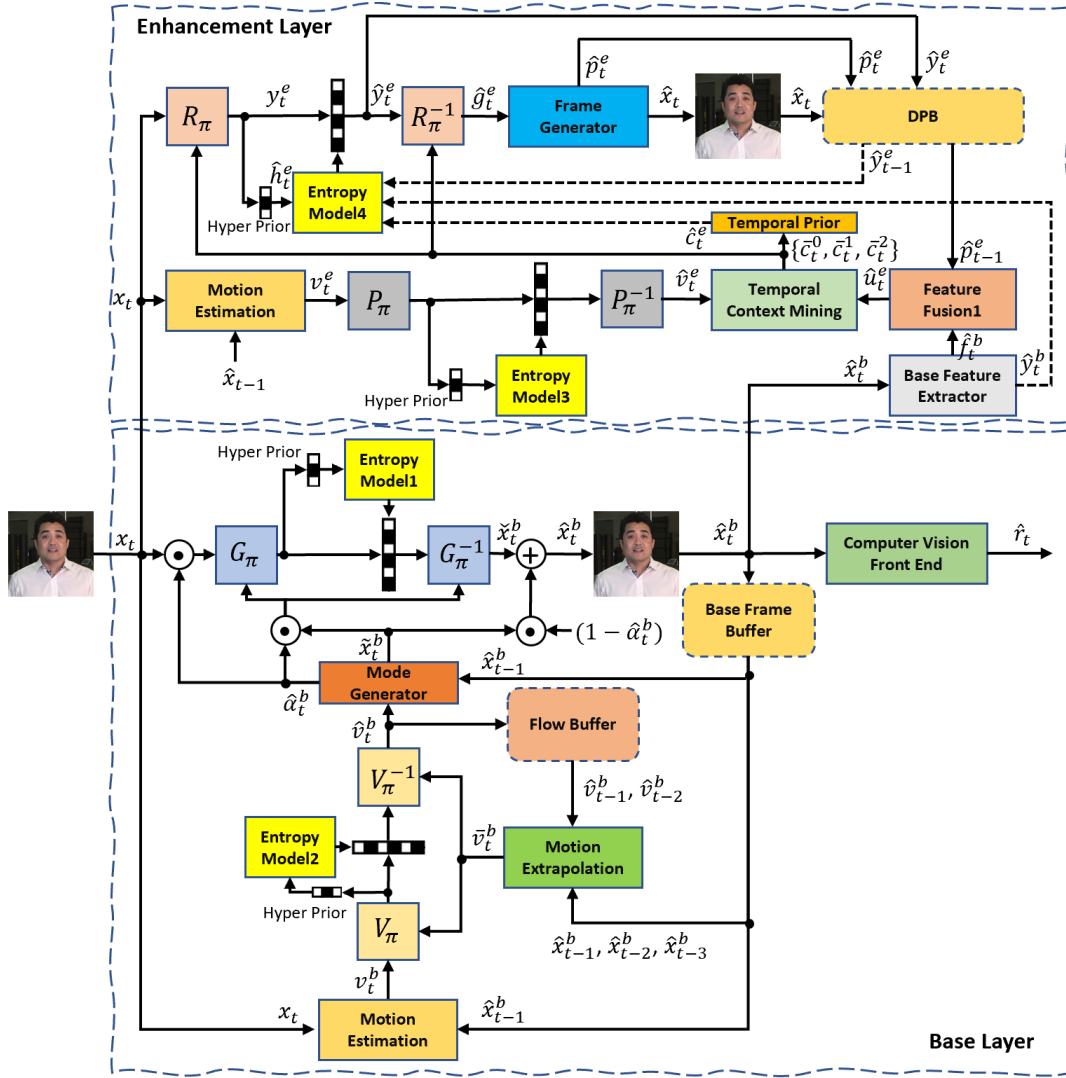


Fig. 2. The block diagram of the proposed learned scalable video compression system. The input video frame is  $x_t$ . The base layer has two outputs: the reconstructed base frame  $\hat{x}_t^b$  and the latent features  $\hat{r}_t$  by which the computer vision task is performed. The enhancement layer has only one output, which is the reconstructed frame  $\hat{x}_t$ .

occasional human viewing (enhancement layer), for cases like emergencies or incident review.

### B. The Base Layer

As shown in Fig. 2, the base layer consists of several components, which are described below.

1) *Motion Estimator and Coder*: Initially, the input video frame,  $x_t$ , and the previously decoded base frame,  $\hat{x}_{t-1}^b$ , are fed into a DNN-based motion estimation network. This network is designed to estimate the optical flow, denoted by  $v_t^b$ , between  $x_t$  and  $\hat{x}_{t-1}^b$ . For this purpose, we use PWC-Net [27]. The flow  $v_t^b$  is then encoded by a DNN-based encoder,  $V_\pi$ , to obtain a compressed motion bitstream in the base layer. This stream is decoded by a DNN-based decoder,  $V_\pi^{-1}$ , to obtain a decoded flow,  $\hat{v}_t^b$ . For this purpose, we adopt the conditional coder from CANF-VC [10], which codes a signal conditioned on its predictor to achieve better rate-distortion performance. To obtain a predictor for conditional coding of  $v_t^b$ , we utilized the motion extrapolation network proposed in

[10]. This network leverages the two previously-decoded flow maps,  $\hat{v}_{t-2}^b$  and  $\hat{v}_{t-1}^b$ , as well as the three previously-decoded base frames,  $\hat{x}_{t-3}^b$ ,  $\hat{x}_{t-2}^b$ , and  $\hat{x}_{t-1}^b$ , to generate a predictor,  $\bar{v}_t^b$ , for  $v_t^b$ .

2) *Motion Compensation*: The optical flow map  $\hat{v}_t^b$  is used to warp the previously-decoded base frame  $\hat{x}_{t-1}^b$  through a motion compensation network to obtain a predictor frame,  $\bar{x}_t^b$ , for conditional coding of the current frame  $x_t$ . Also,  $\hat{v}_t^b$  is stored in a flow buffer to be used for motion extrapolation of the subsequent frames. We used the same motion compensation network as proposed in [10].

3) *Conditional Mode Generator*: To improve the coding performance of the base layer, we used the idea of learned conditional coding modes proposed in our earlier work on learned video coding, called LCCM-VC [24]. Specifically, the previously-reconstructed base frame  $\hat{x}_{t-1}^b$ , the motion-compensated frame  $\bar{x}_t^b$ , and the decoded flow  $\hat{v}_t^b$  are fed to the mode generator from [24] to obtain two weight maps,  $\hat{\alpha}_t^b$  and  $\hat{\beta}_t^b$ . Since these maps are produced from previously



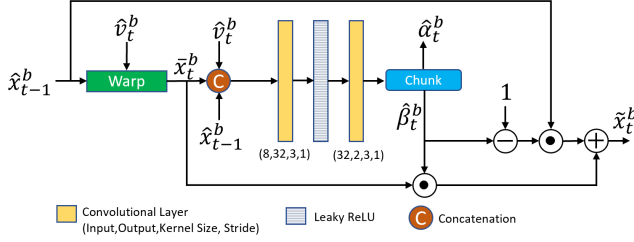


Fig. 3. The structure of the proposed conditional mode generator.

(de)coded data, they can be regenerated at the decoder without any additional bits. Using  $\hat{\beta}_t^b$ , an enhanced predictor,  $\tilde{x}_t^b$ , is generated as follows:

$$\tilde{x}_t^b = \hat{\beta}_t^b \odot \bar{x}_t^b + (\mathbb{1} - \hat{\beta}_t^b) \odot \hat{x}_{t-1}^b, \quad (13)$$

where  $\odot$  denotes Hadamard (element-wise) product and  $\mathbb{1}$  is the all-ones matrix. At each pixel location, the value of  $\tilde{x}_t^b$  is a weighted combination of  $\bar{x}_t^b$  and  $\hat{x}_{t-1}^b$ , where the weight is defined by the corresponding value in  $\hat{\beta}_t^b$ . Hence,  $\tilde{x}_t^b$  is a predictor for the current frame being coded, whose values are adaptively obtained from the previously-reconstructed base frame ( $\hat{x}_{t-1}^b$ ) and the motion-compensated base frame ( $\bar{x}_t^b$ ). After that,  $\tilde{x}_t^b$  is multiplied by  $\hat{\alpha}_t^b$  in a pixel-wise manner, and the obtained result, i.e.  $\hat{\alpha}_t^b \odot \tilde{x}_t^b$ , is fed as a predictor to the inter-frame coder described next. The structure of the proposed conditional mode generator is shown in Fig. 3.

4) *Base Inter-frame Coder*: The predictor  $\hat{\alpha}_t^b \odot \tilde{x}_t^b$  is used for conditional coding of the current frame  $x_t$ . For this purpose, we utilized LCCM-VC [24], which is an extension of CANF-VC [10]. Using this framework, the conditional encoder of the base inter-frame coder,  $G_\pi$ , encodes  $\hat{\alpha}_t^b \odot x_t$  using  $\hat{\alpha}_t^b \odot \tilde{x}_t^b$  to produce a compressed bitstream, which is used to decode an image  $\tilde{x}_t^b$  via  $G_\pi^{-1}$ . Finally, the reconstructed base frame,  $\hat{x}_t^b$ , is generated as follows:

$$\hat{x}_t^b = \tilde{x}_t^b + (\mathbb{1} - \hat{\alpha}_t^b) \odot \tilde{x}_t^b. \quad (14)$$

Note that, for pixels where  $\hat{\alpha}_t^b \rightarrow 0$ ,  $\hat{x}_t^b$  becomes equal to  $\tilde{x}_t^b$ , so the inter-frame coder does not need to code anything. This resembles the SKIP mode in conventional video coders, and depending on the value of  $\hat{\beta}_t^b$ , the system can copy directly from  $\hat{x}_{t-1}^b$ ,  $\bar{x}_t^b$ , or a mixture of these two, to obtain  $\tilde{x}_t^b$ . When  $\hat{\alpha}_t^b \rightarrow \mathbb{1}$ , only the inter-frame coder is used to obtain  $\hat{x}_t^b$ . In the limiting case when  $\hat{\alpha}_t^b \rightarrow \mathbb{1}$  and  $\hat{\beta}_t^b \rightarrow \mathbb{1}$ , LCCM-VC [24] becomes CANF-VC [10]. Hence, as discussed in [24], LCCM-VC has more flexibility and a larger number of conditional coding modes than CANF-VC. The architecture of  $G_\pi$  and  $G_\pi^{-1}$  is similar to that of  $V_\pi$  and  $V_\pi^{-1}$ .

5) *Task-Relevant Feature Extraction*: The obtained base frame,  $\hat{x}_t^b$ , is stored in the base frame buffer for subsequent frame coding and is also fed to the base task network. In our work, this is YOLOv5 [23] for object detection, but in principle any (differentiable) network could be used here for any computer vision task. To enable unsupervised training of the base layer, we truncate the task network and utilize a copy of the resulting front-end of the network within the base layer,

as described next. Specifically, we feed  $\hat{x}_t^b$  to the cloned front-end network in the following manner:

$$\hat{r}_t = F_{\text{trainable}}^{\text{front-end}}(\hat{x}_t^b), \quad (15)$$

where  $F_{\text{trainable}}^{\text{front-end}}(\cdot)$  denotes the cloned front-end network, which is trainable during the training process alongside the rest of the base layer, and  $\hat{r}_t$  is the resultant feature tensor. Then  $\hat{r}_t$  is fed to the back-end part of the original pre-trained task network,  $F_{\text{original}}^{\text{back-end}}(\hat{r}_t)$ , where  $F_{\text{original}}^{\text{back-end}}(\cdot)$  is not trained during the training process.

The primary advantage of this methodology is to eliminate the need for ground-truth labels for the base layer. The amount of labeled data for video (especially uncompressed video, which is needed in our application) is very limited, and it makes sense to use it all for testing. So instead, we train the base layer to match the features  $r_t$  of the pre-trained network at a particular layer, where

$$r_t = F_{\text{original}}^{\text{front-end}}(x_t), \quad (16)$$

and this way, we don't need to use labelled video in training.

The selection of the layer for feature matching will depend on the application constraints. The rate-distortion results in [28], [29] suggest that better performance is achieved when matching deeper layers. However, this requires making  $F_{\text{trainable}}^{\text{front-end}}(\cdot)$  larger, which in turn increases the complexity of the base layer. For the experiments in this study, we chose the first five layers of YOLOv5 as the front-end to demonstrate the performance of the system. In practice, the optimal choice will depend on the computational resources, allowed latency, available bandwidth, etc., in a particular application scenario.

6) *Base Layer Loss Function*: The loss function for training the proposed base layer is defined as follows:

$$L_{\text{base}}(t) = R_{\text{base}}(t) + \lambda_{\text{base}} \text{MSE}(r_t, \hat{r}_t) \quad (17)$$

where MSE is the mean squared error,  $\lambda_{\text{base}}$  is the Lagrange multiplier, and  $R_{\text{base}}(t)$  is the total rate of the base layer for coding  $x_t$ , which is defined as:

$$R_{\text{base}}(t) = R_{\text{base}}^{\text{motion}}(t) + R_{\text{base}}^{\text{signal}}(t), \quad (18)$$

where  $R_{\text{base}}^{\text{motion}}(t)$  is the rate of the motion bitstream produced by coding  $v_t^b$  conditioned on  $\bar{v}_t^b$  plus the rate associated for its hyper prior, and  $R_{\text{base}}^{\text{signal}}(t)$  is the rate for coding  $x_t$  conditioned on  $\tilde{x}_t^b$  plus the rate associated for its hyper prior.

Two visual examples of the decoded base frame ( $\hat{x}_t^b$ ) in the trained system are shown in Fig. 4 for two different rates, along with the original frames ( $x_t$ ) and the residual ( $x_t - \hat{x}_t^b$ ). As is evident from the residual frames in this figure, the base frame omits certain details of the original frame, which are deemed unnecessary for the object detection task, in order to curtail the rate. Consequently, the base layer can be encoded at a significantly lower rate than the original frame.

### C. The Enhancement Layer

To implement the enhancement layer of the proposed system, we used the conditional coding-based framework proposed in [14] as the basis. However, we made some modifications to fit it into our scalable codec, as will be discussed in the following subsections. The components of the enhancement layer are shown in Fig. 2 and described below.

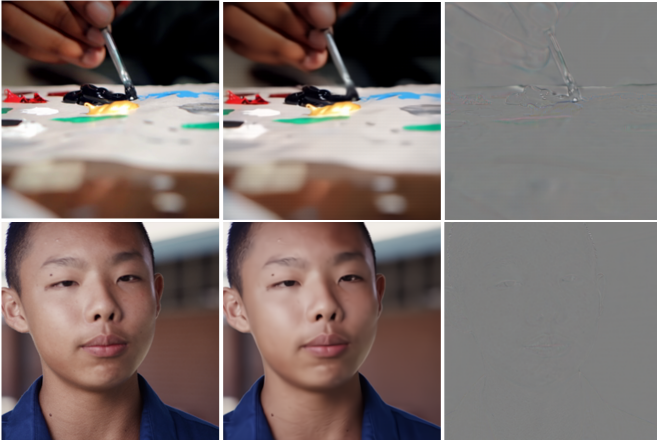


Fig. 4. Two visual examples of the base frame at two different rates (top row: 0.01 bpp, bottom row: 0.10 bpp). The original frame  $x_t$  (left), base frame  $\hat{x}_t^b$  (middle), and the residual  $x_t - \hat{x}_t^b$  (right).

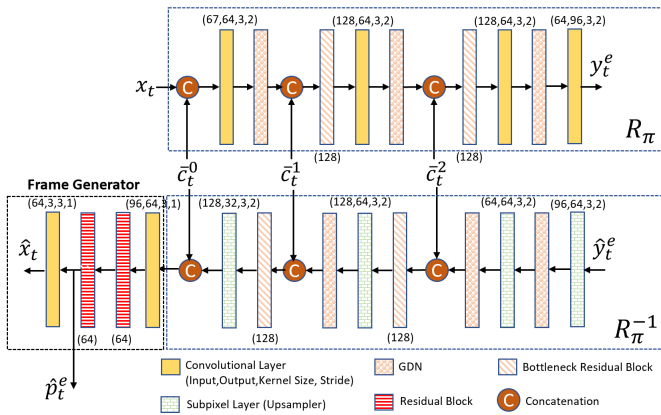


Fig. 5. The structure of the context encoder  $R_\pi$ , the context decoder  $R_\pi^{-1}$ , and the frame generator.

1) *Context Encoder*: The current frame  $x_t$  is first encoded by a conditional context encoder,  $R_\pi$ , to produce a latent representation  $y_t^e$ . The conditional context encoder uses three temporal contexts  $\{\hat{c}_t^0, \hat{c}_t^1, \hat{c}_t^2\}$  for conditional coding of  $x_t$ . These contexts are produced by a temporal context mining (TCM) network, which is described in Section III-C5. The structure of the context encoder is shown in Fig. 5. The obtained latent representation  $y_t^e$  is then quantized and compressed by an arithmetic encoder whose symbol probabilities are estimated by a hyper prior-based entropy model [6]. Using this approach, a compressed context bitstream is produced along with a side compressed bitstream for signaling the hyper-priors  $h_t^e$ . The entropy model is described in Section III-C6 below.

2) *Context Decoder*: The resultant context bitstream is then decompressed at the decoder by an arithmetic decoder to obtain  $\hat{y}_t^e$ , which is then fed to a conditional context decoder,  $R_\pi^{-1}$ . Similarly, the hyper-priors of the current frame are decoded from the side bitstream to obtain the temporal hyper-prior  $\hat{h}_t^e$ . A copy of  $\hat{y}_t^e$  is stored in the generalized decoded picture buffer (DPB) to be used for encoding the subsequent frames.  $R_\pi^{-1}$  uses the three temporal contexts and transforms  $\hat{y}_t^e$  into a new latent representation  $\hat{g}_t^e$ , which is then fed to

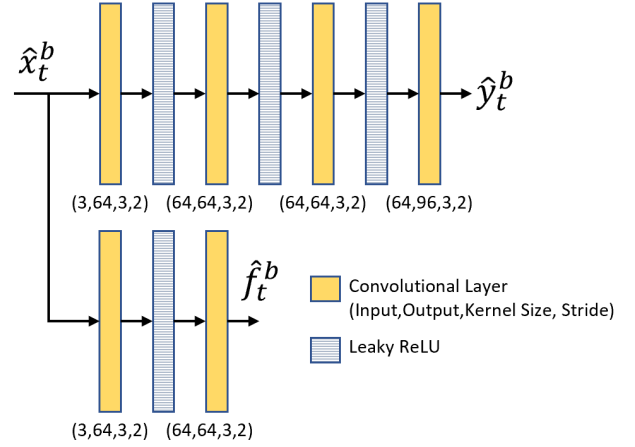


Fig. 6. The structure of the base feature extractor network.

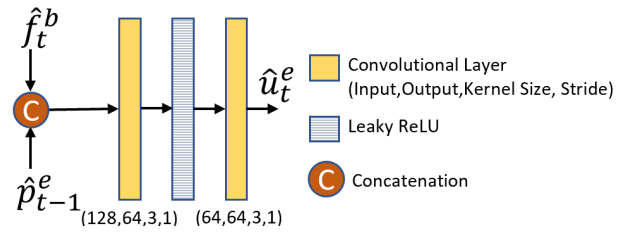


Fig. 7. The structure of the first feature fusion network.

the frame generator to reconstruct the transmitted frame, as will be described next. The structure of the context decoder is shown in Fig. 5

3) *Frame Generator*: The frame generator passes its input tensor  $\hat{g}_t^e$  through a number of convolutional layers and residual blocks as in [14], and reconstructs the input frame as  $\hat{x}_t$ . The output of the layer before the last layer in the frame generator,  $\hat{p}_t^e$ , is also stored in the DPB along with  $\hat{x}_t$ . The feature tensor  $\hat{p}_t^e$  is subsequently used by the TCM network to produce the temporal contexts.

4) *Motion Estimator and Coder*: The current frame  $x_t$  and the previously-reconstructed frame in the enhancement layer,  $\hat{x}_{t-1}$ , are fed to a motion estimation network to estimate a flow map,  $v_t^e$ , in the enhancement layer. Similar to the base layer, we also use PWC-Net [27] for motion estimation in the enhancement layer. The estimated flow map is then coded by a hyper-prior-based encoder [6],  $P_\pi$ , to obtain the compressed motion bitstream in the enhancement layer. The motion bitstream is then decoded by the corresponding hyper-prior-based decoder,  $P_\pi^{-1}$ , to obtain the decoded flow map,  $\hat{v}_t^e$ , which provides an estimated motion vector for each pixel within the current frame in the enhancement layer.

5) *Temporal Context Mining*: To generate the temporal contexts to encode the current frame, the decoded base frame  $\hat{x}_t^b$  is first fed to a base feature extractor network to obtain two output feature tensors:  $\hat{f}_t^b$  and  $\hat{y}_t^b$ . The structure of the base feature extractor is shown in Fig. 6. The first feature tensor,  $\hat{f}_t^b$ , is then fused with the features of the previous frame reconstructed by the frame generator,  $\hat{p}_{t-1}^e$ , to generate a new feature tensor  $\hat{u}_t^e$ . The feature fusion is performed by a simple network with two convolutional layers whose

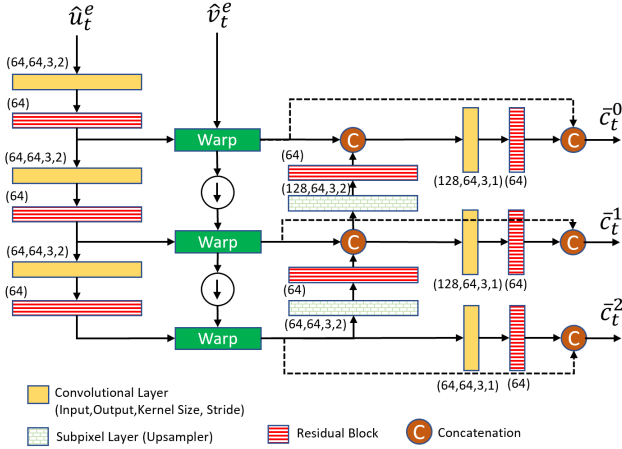


Fig. 8. The structure of the temporal context mining (TCM) network.

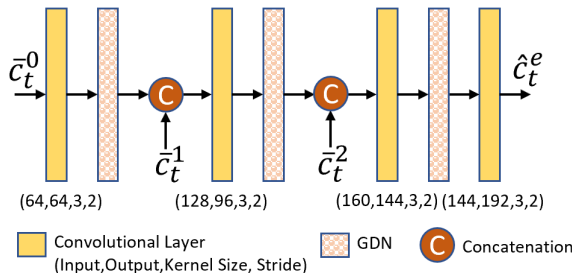


Fig. 9. The structure of the temporal prior network.

structure is shown in Fig. 7. After that,  $\hat{u}_t^e$  and the decoded flow map  $\hat{v}_t^e$  are fed to the temporal context mining (TCM) network proposed in [14]. The structure of TCM is shown in Fig. 8. TCM uses  $\hat{v}_t^e$  and warps  $\hat{u}_t^e$  at three different scales to obtain three contexts  $\{\hat{c}_t^0, \hat{c}_t^1, \hat{c}_t^2\}$ , each at a different scale. These contexts provide rich temporal information for coding the current frame in the enhancement layer. After that, these three contexts are combined through a temporal prior network whose structure is shown in Fig. 9. The output of this network is  $\hat{c}_t^e$ , which conveys the temporal context of the current frame. The second output of the base feature extractor,  $\hat{y}_t^b$ , is used by the entropy model, which is described next. In [14],  $\hat{p}_{t-1}^e$  is used directly as input to the TCM module. However, in our design, we fuse  $\hat{p}_{t-1}^e$  with  $\hat{f}_t^b$  through the feature fusion network, and the resulting output,  $\hat{u}_t^e$ , is used as input to the TCM module. In this way, the generated temporal contexts leverage the information provided in both the base frame and the previous reconstructed frame in the enhancement layer.

6) *Entropy Model:* Similar to [14] and [9], we use the factorized entropy model for the hyper-prior coder, and the Laplace distribution to model the quantized latent representations in the enhancement layer,  $\hat{y}_t^e$ . However, to improve the performance of the entropy model, we fuse the hyper priors of the current frame,  $\hat{h}_t^e$ , with the temporal prior  $\hat{c}_t^e$ , decoded latents from the previous enhancement frame  $\hat{y}_{t-1}^e$  and base features of the current frame  $\hat{y}_t^b$  through an entropy parameter estimation network. In [14], only the hyper-prior  $\hat{h}_t^e$  and the temporal prior  $\hat{c}_t^e$  are fed to the entropy model. However, in our design, in addition to  $\hat{h}_t^e$  and  $\hat{c}_t^e$ , we also feed  $\hat{y}_t^b$  and  $\hat{y}_{t-1}^e$

to the entropy model to enrich its input information. Moreover, we add the attention layer so the system can learn where to take the relevant information for entropy modelling.

The structure of the entropy model is shown in Fig. 10. As shown in this figure, the hyper-prior  $\hat{h}_t^e$  and the temporal prior  $\hat{c}_t^e$  are first concatenated, and fed to three consecutive convolutional layers. The resulting feature tensor is then concatenated with  $\hat{y}_{t-1}^e$  and  $\hat{y}_t^b$ , and the generated tensor is fed to two consecutive convolutional layers followed by an attention layer. The output of the attention layer is then chunked in half to produce two tensors,  $\hat{\mu}_t^e$  and  $\hat{\sigma}_t^e$ , which are used to estimate the mean and variance of the Laplace distribution, respectively.

Sample frames from the BasketballDrill sequence (HEVC Class C) are also shown in Fig. 10:  $x_t$  is the current (to-be-coded) frame at time  $t$ ,  $\hat{x}_{t-1}^e$  is the previously decoded frame in the enhancement layer, and  $\hat{x}_t^b$  is the base frame at time  $t$ . To gain insight into the operation of the entropy model, visualizations of the corresponding latent features are also shown. As seen in these sample visualizations, incorporating the attention layer into the proposed entropy parameter estimation network facilitates its ability to selectively focus on important features within the input data, resulting in more efficient parameter estimation. For instance, the attention mechanism weakens static areas that correspond to the floor in the first channel of  $\hat{\sigma}_t^e$ ; since these areas are static,  $\hat{\sigma}_t^e$  reduces towards zero, while it remains higher near moving objects, the basketball and players. We can also observe that some parts of the last channel of  $\hat{\mu}_t^e$  are mostly obtained from the last channel of the base features  $\hat{y}_t^b$  (e.g., those in the solid circle) while some other parts (e.g., those in the dashed circle) are mostly taken from the enhancement features of the previous frame,  $\hat{y}_{t-1}^e$ . By utilizing attention and feeding it both the base and previous enhancement features, the entropy model is able to leverage the information available in the current base frame as well as previously-reconstructed frames in the enhancement layer, thereby enhancing its ability to achieve better compression of the current enhancement frame.

As will be discussed in the following section, the base and enhancement layers are trained on sequences of contiguous frames to allow the models to learn temporal relationships. Specifically, the gradients of the current frame are back-propagated to the reference frames that preceded it within a temporal window of length  $N$  frames. As a result, the tensors  $\hat{y}_{t-1}^e$ ,  $\hat{y}_t^b$  and  $\hat{c}_t^e$  are endowed with substantial information not only from the current frame, but also from the preceding frames. This characteristic enables the system to take advantage of the correlations among the latent representations of multiple frames to model the entropy more effectively.

Having obtained  $\hat{\mu}_t^e$ ,  $\hat{\sigma}_t^e$ , and  $\theta_t^e = \{\hat{h}_t^e, \hat{c}_t^e, \hat{y}_{t-1}^e, \hat{y}_t^b\}$ , the formulation for the conditional distribution of the latent representations can be obtained as follows [6]:

$$p_{\hat{y}_t^e | \theta_t^e}(\hat{y}_t^e | \theta_t^e) = \prod_i p_{\hat{y}_t^e | \theta_t^e}(\hat{y}_{t,i}^e | \theta_t^e), \quad (19)$$



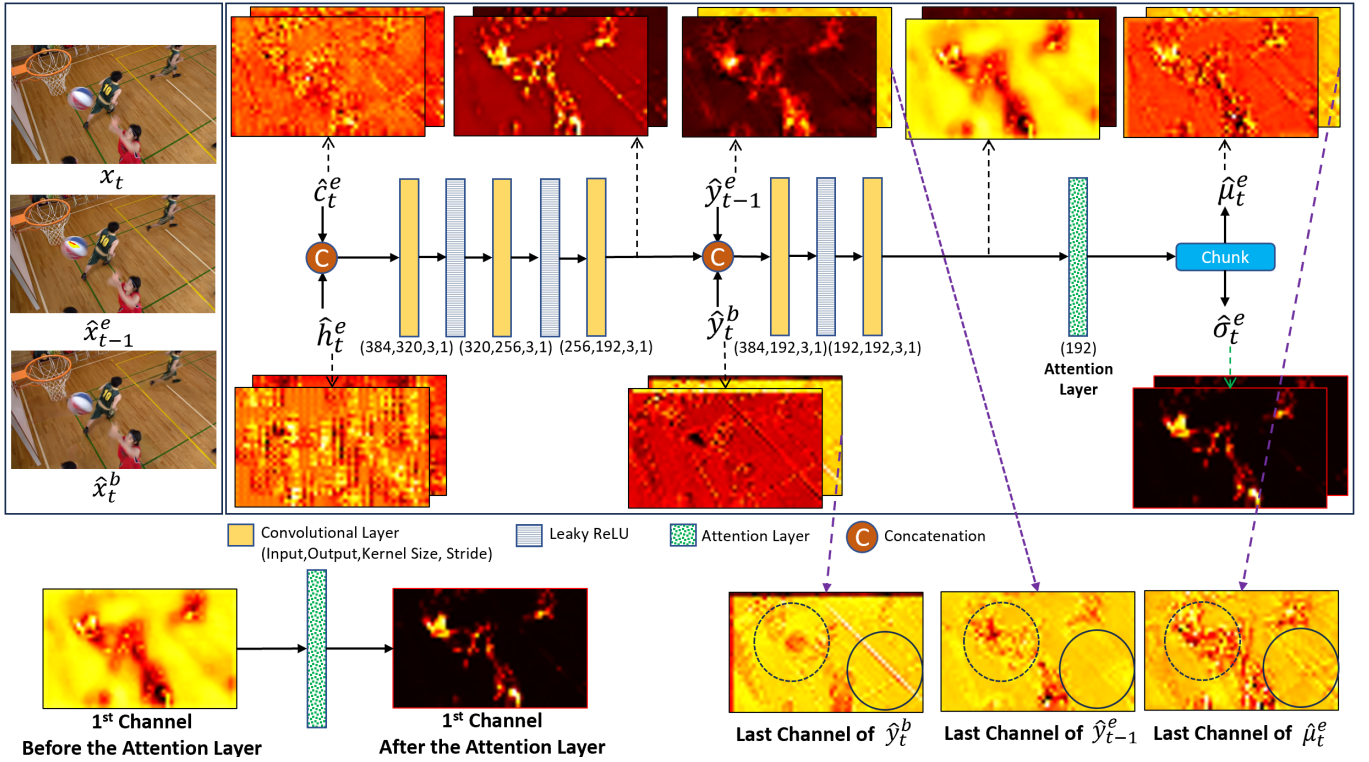


Fig. 10. The structure of the proposed entropy parameter estimation network. The latent feature maps are shown for a sample frame from BasketballDrill (HEVC Class C).

where the index  $i$  represents the spatial location, and

$$\begin{aligned} p_{\hat{y}_t^e|\theta_t^e}(\hat{y}_{t,i}^e|\theta_t^e) &= \left[ \mathcal{L}(\hat{\mu}_{t,i}^e, \hat{\sigma}_{t,i}^e) * \mathcal{U}\left(-\frac{1}{2}, \frac{1}{2}\right) \right] (\hat{y}_{t,i}^e) \\ &= \text{cdf}\left(\hat{y}_{t,i}^e + \frac{1}{2}\right) - \text{cdf}\left(\hat{y}_{t,i}^e - \frac{1}{2}\right), \end{aligned} \quad (20)$$

where  $\mathcal{L}(\hat{\mu}_{t,i}^e, \hat{\sigma}_{t,i}^e)$  represents the Laplacian probability density function with mean  $\hat{\mu}_{t,i}^e$  and variance  $\hat{\sigma}_{t,i}^e$ ,  $*$  represents the convolution,  $\mathcal{U}(-\frac{1}{2}, \frac{1}{2})$  represents the uniform probability density in the range  $[-\frac{1}{2}, \frac{1}{2}]$  (which models uniform quantization), and  $\text{cdf}(\cdot)$  is the cumulative distribution function (CDF) of the resulting distribution. The estimated per-sample rate for coding  $\hat{y}_t^e$  is given by  $-\log_2(p_{\hat{y}_t^e|\theta_t^e}(\hat{y}_t^e|\theta_t^e))$ , and the estimated entropy is the expectation of this quantity. This rate estimate is one of the loss terms used for training the enhancement layer, as discussed next.

7) *Enhancement Layer Loss Function*: The loss function for the enhancement layer is defined as:

$$L_{enh}(t) = R_{enh}(t) + \lambda_{enh} \text{MSE}(x_t, \hat{x}_t), \quad (21)$$

where  $\lambda_{enh}$  is the Lagrange multiplier, and  $R_{enh}(t)$  is the rate estimate for coding the current enhancement-layer frame, which is defined as follows:

$$R_{enh}(t) = R_{enh}^{\text{motion}}(t) + R_{enh}^{\text{context}}(t), \quad (22)$$

where  $R_{enh}^{\text{motion}}(t)$  is the total rate estimate for coding the motion information in the enhancement layer and  $R_{enh}^{\text{context}}(t) = \mathbb{E}[-\log_2(p_{\hat{y}_t^e|\theta_t^e}(\hat{y}_t^e|\theta_t^e))]$ .

## IV. EXPERIMENTS

In this section, we describe the experiments performed to evaluate the performance of the proposed scalable video codec. Training details are described in Section IV-A, followed by the evaluation methodology in Section IV-B, and the experimental results for the base and enhancement layers in Sections IV-C and IV-D, respectively. Break-even analysis is presented in Section IV-E.

### A. Training

For training the proposed system, we used the VIMEO-90K Setuplet dataset [30], which consists of 91,701 7-frame sequences with fixed resolution  $448 \times 256$ , extracted from 39K selected video clips. We randomly cropped these clips into  $256 \times 256$  patches and used them to train the system. We used Adam [31] optimizer with batch size of 4. We employed a training strategy commonly used in recent papers [32], [10], [14], where the video codec is trained on a group of consecutive frames. In general, utilizing a larger group of frames in training can lead to better results. However, similar to [10], [14] and motivated by memory constraints, in our experiments the loss function for each layer is computed over  $N = 5$  consecutive frames as follows:

$$L_{base}^* = \frac{1}{N} \sum_{t=1}^N L_{base}(t), \quad L_{enh}^* = \frac{1}{N} \sum_{t=1}^N L_{enh}(t), \quad (23)$$

where  $L_{base}(t)$  and  $L_{enh}(t)$  are defined as in (17) and (21), respectively. Using this training strategy, the gradients of each frame are back-propagated towards other frames in the group,

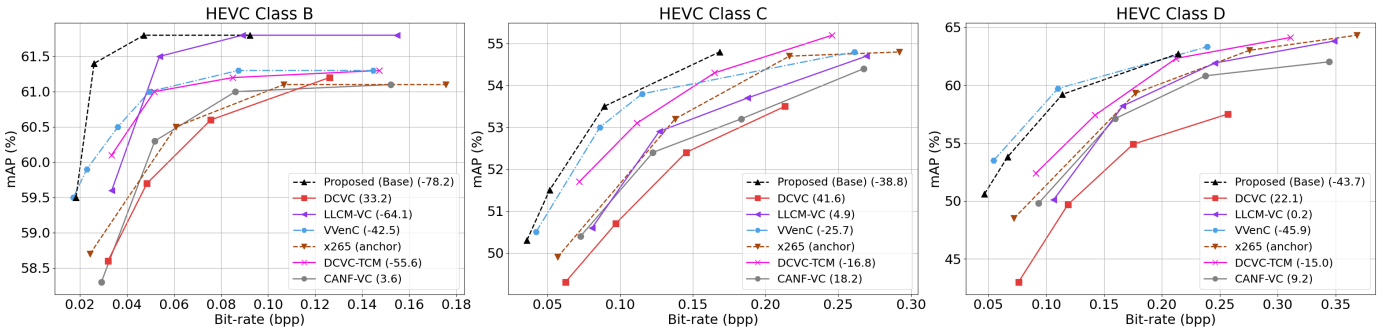


Fig. 11. Comparing the performance of various methods in the base layer terms of mAP (%) on three datasets. In the legend of each graph, the BD-Rate(%) of the corresponding method is also shown with respect to x265 (anchor).

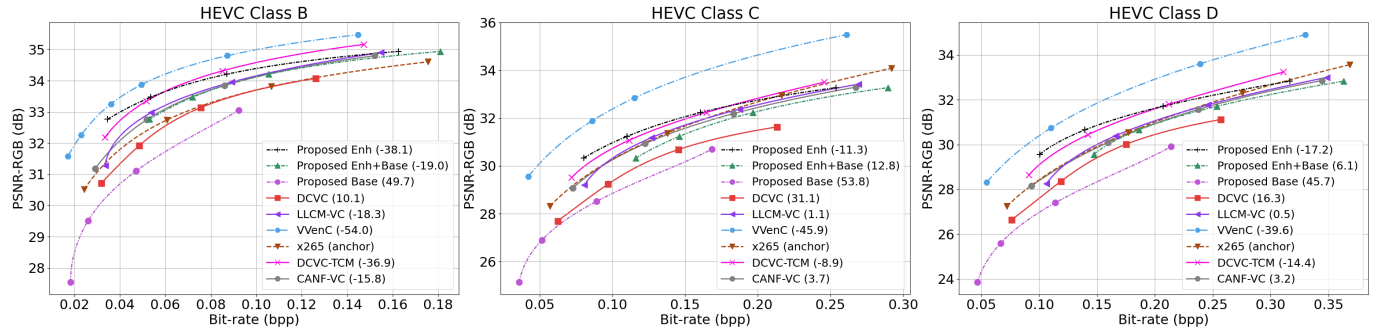


Fig. 12. Comparing the RD performance of various methods in terms of RGB-PSNR (dB) on three datasets. In the legend of each graph, the BD-Rate(%) of the corresponding method is also shown with respect to x265 (anchor).

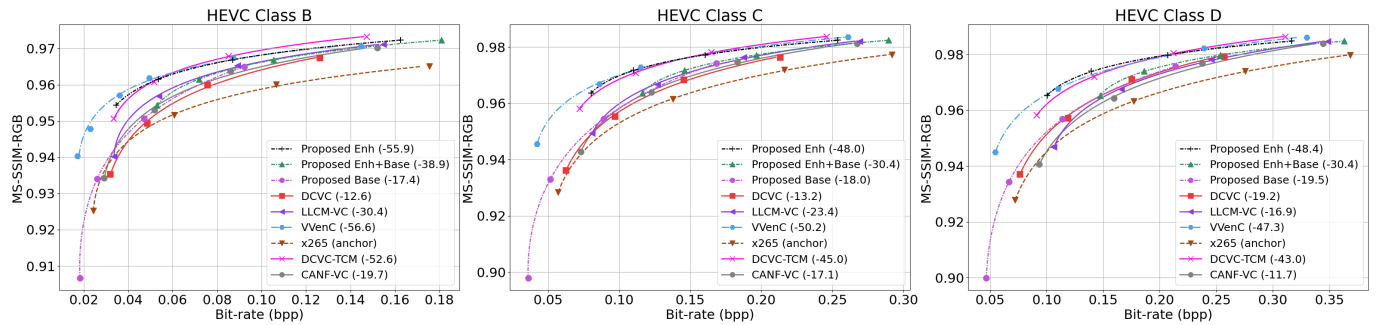


Fig. 13. Comparing the RD performance of various methods in terms of RGB-MS-SSIM on three datasets. In the legend of each graph, the BD-Rate(%) of the corresponding method is also shown with respect to x265 (anchor).

which allows the system to capture temporal relationships among a group of consecutive frames.

For the base layer, we used  $\lambda_{base} \in \{2, 4, 8, 16\}$ . All networks in the base layer were first initialized with their pre-trained weights from [10]. For YOLOv5, we used the PyTorch implementation provided in [33], and used the checkpoint for the “small” model for the initialization. The learning rate was set to a small value  $10^{-6}$ , and the entire layer was trained end-to-end for 10 epochs. We first trained the base layer, and then kept it frozen during the training of the enhancement layer.

For the enhancement layer, we used  $\lambda_{enh} \in \{256, 512, 1024, 2048\}$ . The learning rate was set to  $10^{-4}$  for the first 5 epochs, and then reduced to  $10^{-5}$  for the next 10 epochs. We first trained the enhancement layer with  $\lambda_{enh} = 2048$  (highest rate), then all lower-rate models were initialized from this model.

## B. Evaluation Methodology

To evaluate a video codec intended for both object detection and input frame recovery, it is necessary to test it on datasets consisting of raw (uncompressed) video and associated object labels. To our knowledge, only two such datasets are currently available – SFU-HW-Objects-v1 [34] and TVD [35] – and both are being used in the MPEG-VCM standardization effort [16]. The SFU-HW-Objects-v1 dataset is based on raw YUV420 video sequences that were used in the development of video coding standards such as HEVC [4] and VVC [5]. Each sequence contains between 240–600 frames. A subset of these sequences was labeled with COCO7-style object labels. The TVD dataset includes 86 sequences, each consisting of 65 frames. However, object labels are only provided for 55 unique video triplets (3-frame sequences).

We used the following video codecs as benchmarks: x265



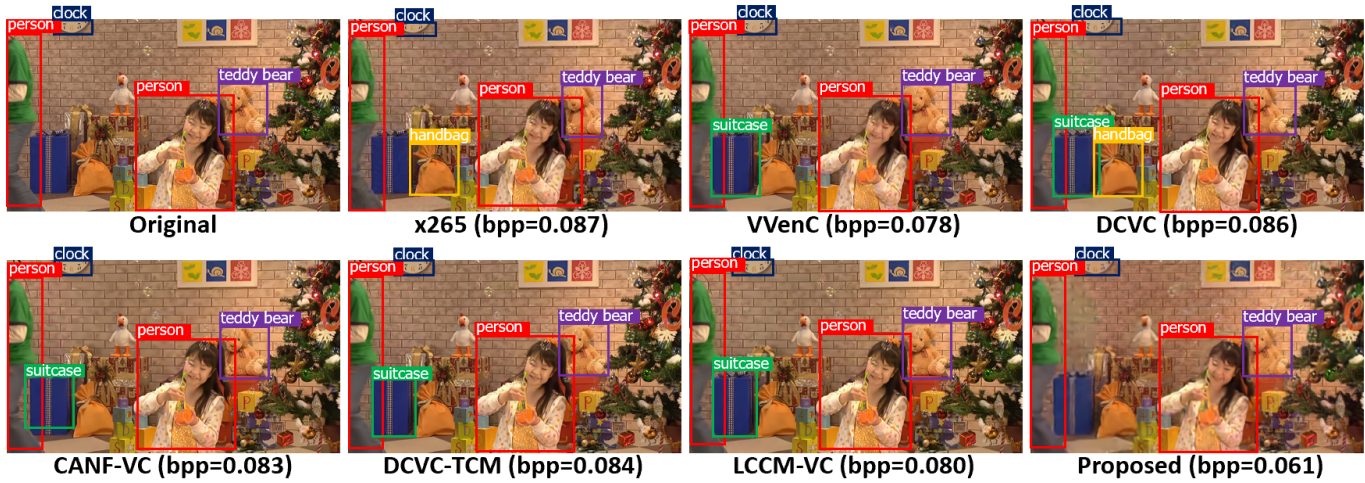


Fig. 14. Comparing the object detection performance of various methods on a sample frame from PartyScene (HEVC Class C). The ground-truth object labels come from the SFU-HW-Objects-v1 dataset.



Fig. 15. Comparing the input reconstruction performance of various methods on a patch from a sample frame of RaceHorses (HEVC Class C). The (bpp, PSNR, MS-SSIM) for x265, VVenC, DCVC, CANF-VC, DCVC-TCM, LCCM-VC, the proposed method (Base+Enh), and the proposed method (Enh) is (0.43,33.56,0.9751), (0.43,33.92,0.9802), (0.44,32.65,0.9678), (0.42,33.50,0.9750), (0.43,33.61,0.9760), (0.44,33.78,0.9771), (0.42,33.60,0.9758), and (0.37,33.60,0.9758), respectively. Note that the proposed Enh and the proposed Base+Enh produce the same frame – indicated by “Proposed” in the figure – only the bits are counted differently.

(‘very slow’ mode) [36], VVenC (v1.8.0) [37] with LDP profile (randomaccess\_slow.cfg), DCVC-TCM [14], CANF-VC [10], and DCVC [9]. Among these, x265 was chosen as the anchor against which all other codecs are compared. For x265, which is an efficient implementation of HEVC [4], the quantization parameter (QP) values were {27, 29, 32, 38}. For VVenC, which is an efficient implementation of VVC [5], QP values were {22, 24, 27, 29}. The internal color space for x265 and VVenC was YUV420 (8 bit). Also, four reference frames were used for motion estimation in these conventional codecs. However, all the tested learned codecs (CANF-VC, DCVC-TCM, LCCM-VC, DCVC, and the proposed method) use only one reference frame in their optical flow estimators. As reported in [14], if we use only one reference frame for

the conventional codecs instead of four, their performance will be degraded considerably. In the experiments, we set the IntraPeriod (also known as Group Of Pictures, GOP) to 32 for all codecs when testing them on SFU-HW-Objects-v1. On the TVD dataset, the GOP size is set to 3 because sequences are 3-frames long.

Following the existing practice in the learned video coding literature [10], [38], [9], [14], to evaluate the performance of various codecs, the bitrates were measured in bits per pixel (bpp) and the frame reconstruction quality was measured by RGB Peak Signal-to-Noise Ratio (RGB-PSNR) and RGB Multi-Scale Structural Similarity Index Metric (RGB-MS-SSIM) [39]. Object detection accuracy was measured by Mean Average Precision (mAP) [25]. Following the methodology

used in MPEG-VCM [16], these quantities can be agglomerated into a single numerical score called Bjøntegaard Delta Rate (BD-Rate) [40], which computes the average bitrate difference between two codecs at the equivalent quality level, where the quality may be measured by PSNR, MS-SSIM, or mAP, as the case may be. So, for example, if a certain codec achieves  $-10\%$  BD-Rate-mAP relative to a given anchor, it means that it achieves, on average,  $10\%$  bitrate reduction relative to the anchor while producing the same mAP.

### C. Object Detection Performance

First, we evaluate the object detection performance. For the proposed codec, we only need to decode the base-layer bitstream and feed it to the pre-trained YOLOv5 back-end. For other codecs, we decode each frame and then feed it to the pre-trained YOLOv5. Fig. 11 shows the mAP (%) vs. bitrate (bpp) on the three classes of sequences from the SFU-HW-Objects-v1 dataset. The legend in each graph shows BD-Rate-mAP percentage in the brackets, relative to the x265 anchor. Negative values indicate bit savings relative to the anchor at the equivalent mAP. BD-Rate-mAP results are also summarized in Table I, where the best result in each row is highlighted in bold. The table also includes the results on the TVD dataset. However, since the sequences in the TVD dataset are short (3 frames each), the performance of most codecs is similar; the performance of most codecs  $-14.6\%$  BD-Rate-mAP relative to x265. The TVD sequences seem too short to allow distinguishing the various codecs' ability to capture long-range relationships among features relevant to object detection. The last two rows in Table I show the average BD-Rate-mAP results, averaged according to the number of frames in each dataset. We see that the overall performance (bottom row) is dominated by the performance on SFU-HW-Objects-v1, since this dataset has many more frames than TVD. Overall, the results indicate that the proposed codec outperforms all other codecs. VVenC comes as the second best, followed by DCVC-TCM.

Fig. 14 provides a visual example of object detection on a sample frame from the PartyScene sequence (HEVC Class C). In this figure, we show the bounding box of the detected objects overlaid on the reconstructed frame. For the proposed method, we show the base frame because only base-layer information is used. As seen in this example, the proposed method is capable of achieving better detection accuracy at a lower rate compared to other methods. Specifically, we note that in the frames produced by other codecs, the gift box is often mis-detected as a suitcase, and the gift bag is confused with a handbag. While these objects might be similar to some extent, the compression artifacts introduced by other codecs cause the detector to produce incorrect detections, whereas our method preserves the relevant features well, avoiding misclassification even at lower rates than other methods.

### D. Frame Reconstruction Performance

When it comes to the performance of reconstructing compressed frames for human viewing, the situation is straightforward for conventional video codecs, whether learned or

handcrafted: we simply decode the compressed bitstream, generate the decoded frames, and measure their quality using an appropriate metric (PSNR or MS-SSIM in this work). However, for the proposed codec, there are several options.

First, note that the base layer of the proposed system generates video frames and stores them in the base frame buffer, as shown in Fig. 2. Such frames are intended for object detection rather than human viewing; they preserve enough information to detect objects at low rates, but lack the details that are deemed irrelevant for this task, as illustrated in Fig. 4. Nevertheless, we could ask what their quality is in terms of frame reconstruction metrics. In Figs. 12-13, we refer to this approach as **“Proposed Base”** and in Tables II-III as simply **“Base.”** In this case, only the base-layer bitrate is counted, since base frames are generated from the base-layer bitstream only.

The intended use of the proposed codec is in a closed-loop automated analytics system, where analysis is performed using object detection (base layer) information, and frame reconstruction is initiated depending on the results of the base-layer analysis. For example, in a traffic monitoring system, object detection runs continuously. When the arrangement of detected objects suggests a traffic violation, the enhancement layer is turned on to provide additional information for frame reconstruction and human viewing. Hence, given that base-layer information is already available at the analysis server, only the enhancement layer bitstream needs to be communicated to provide high-quality frame reconstruction. The bitrate in this case is the enhancement-layer bitrate, and the frame quality is measured on the enhancement-layer frames. This approach is termed **“Proposed Enh”** in Figs. 12-13 and simply **“Enh”** in Tables II-III. It is worth noting that the MPEG-VCM evaluation framework [41] suggests comparing this approach against conventional coding approaches. The goal of MPEG-VCM is stated as [41]: *“The bitrate of the additional compressed bitstream shall be less than the bitrate of the bitstream at similar quality as measured by PSNR, which is the output of the VVC encoding of the unprocessed video.”*

Finally, we can also count the total bitrate (base + enhancement layer) for the proposed codec, along with enhancement-layer frame quality. This is referred to as **“Proposed Base+Enh”** in Figs. 12-13 and simply **“Base+Enh”** in Tables II-III. It is debatable whether the comparison of conventional coding against this case is realistic. Such a comparison may make sense if we knew *in advance* that a situation of interest (e.g., traffic violation in our earlier example) would occur at some point in time, without performing any visual analysis. In such a case, our codec would still have to encode both base and enhancement layer bitstreams, even though the result of the analysis is apparently known ahead of time. Nevertheless, we included these “oracle-style” results for completeness, even though they show less favorable performance of our codec.

Fig. 12 shows the RGB-PSNR (in dB) versus bitrate for various cases on the three classes of HEVC video sequences. The legend shows BD-Rate-PSNR (%) relative to x265 in the brackets. These results are also tabulated in Table II, along with BD-Rate-PSNR on the TVD dataset. As seen from these results, for the input frame reconstruction task, the best-

TABLE I  
OBJECT DETECTION PERFORMANCE IN TERMS OF BD-RATE-MAP (%) ON DIFFERENT DATASETS. THE ANCHOR IS X265.

| Dataset                          | VVenC [37]   | CANF-VC [10] | DCVC-TCM [14] | LCCM-VC [24] | DCVC [9] | Proposed     |
|----------------------------------|--------------|--------------|---------------|--------------|----------|--------------|
| SFU-HW-Objects-v1 (HEVC Class B) | -42.5        | +3.6         | -55.6         | -64.1        | +33.2    | <b>-78.2</b> |
| SFU-HW-Objects-v1 (HEVC Class C) | -25.7        | +18.2        | -16.8         | +4.9         | +41.6    | <b>-38.8</b> |
| SFU-HW-Objects-v1 (HEVC Class D) | -42.4        | +9.2         | -15.0         | +0.2         | +22.1    | <b>-43.7</b> |
| TVD                              | <b>-14.6</b> | -14.3        | <b>-14.6</b>  | <b>-14.6</b> | +18.3    | <b>-14.6</b> |
| Average (SFU-HW-Objects-v1)      | -37.0        | +10.1        | -29.9         | -21.0        | +32.3    | <b>-54.3</b> |
| Average                          | -36.4        | +9.4         | -29.5         | -20.9        | +32.0    | <b>-53.2</b> |

TABLE II  
FRAME RECONSTRUCTION PERFORMANCE IN TERMS OF BD-RATE-PSNR (%) ON DIFFERENT DATASETS. THE ANCHOR IS X265. THE LAST THREE COLUMNS FROM THE RIGHT SHOW THE RESULTS OF THE THREE CASES OF THE PROPOSED METHOD.

| Dataset        | VVenC [37]   | CANF-VC [10] | DCVC-TCM [14] | LCCM-VC [24] | DCVC [9] | Base  | Enh   | Base+Enh |
|----------------|--------------|--------------|---------------|--------------|----------|-------|-------|----------|
| HEVC Class B   | <b>-54.0</b> | -15.8        | -36.9         | -18.3        | +10.1    | +49.7 | -38.1 | -19.0    |
| HEVC Class C   | <b>-45.9</b> | +3.7         | -8.9          | +1.1         | +31.1    | +53.8 | -11.3 | +12.8    |
| HEVC Class D   | <b>-39.6</b> | +3.2         | -14.4         | +0.5         | +16.3    | +45.7 | -17.2 | +6.1     |
| TVD            | <b>-26.3</b> | -0.1         | +4.2          | -1.7         | -0.6     | +55.4 | -7.8  | +17.6    |
| Average (HEVC) | <b>-46.7</b> | -3.4         | -20.6         | -6.0         | +18.9    | +49.7 | -22.7 | -0.6     |
| Average        | <b>-46.2</b> | -3.3         | -19.9         | -5.9         | +18.4    | +49.9 | -22.3 | -0.1     |

TABLE III  
FRAME RECONSTRUCTION PERFORMANCE IN TERMS OF BD-RATE-MS-SSIM (%) ON DIFFERENT DATASETS. THE ANCHOR IS X265. THE LAST THREE COLUMNS FROM THE RIGHT SHOW THE RESULTS OF THE THREE CASES OF THE PROPOSED METHOD.

| Dataset        | VVenC [37]   | CANF-VC [10] | DCVC-TCM [14] | LCCM-VC [24] | DCVC [9] | Base  | Enh          | Base+Enh |
|----------------|--------------|--------------|---------------|--------------|----------|-------|--------------|----------|
| HEVC Class B   | <b>-56.6</b> | -19.7        | -52.6         | -30.4        | -12.6    | -17.4 | -55.9        | -38.9    |
| HEVC Class C   | <b>-50.2</b> | -17.1        | -45.0         | -23.4        | -13.2    | -18.0 | -48.0        | -30.4    |
| HEVC Class D   | -47.3        | -11.7        | -43.0         | -16.9        | -19.2    | -19.5 | <b>-48.4</b> | -30.4    |
| TVD            | -28.0        | -14.2        | -20.4         | -15.4        | -21.6    | +10.2 | <b>-29.3</b> | -13.5    |
| Average (HEVC) | <b>-51.5</b> | -16.3        | -47.0         | -23.8        | -14.9    | -18.3 | -50.9        | -33.4    |
| Average        | <b>-50.9</b> | -16.2        | -46.3         | -23.5        | -15.1    | -17.5 | -50.3        | -32.3    |

TABLE IV  
THE BREAK-EVEN POINT  $\phi$  AGAINST VVENC.

| Frame quality metric | Proposed Enh | Proposed Base+Enh |
|----------------------|--------------|-------------------|
| RGB-PSNR             | 0.41         | 0.27              |
| RGB-MS-SSIM          | 0.97         | 0.47              |

performing method is VVenC followed by our proposed Enh and then DCVC-TCM. The gap between VVenC and our Enh is over 20%. This is not surprising, given that conventional video codecs are known to perform very well on the PSNR metric. It is interesting to note that even though our Base method uses the base layer bitstream only (seemingly a low bitrate), it performs the worst among all the methods tested in Table II. This is because BD-Rate-PSNR between a given codec and the anchor is measured at the equivalent PSNR, and our Base method needs a lot of bits to reach the equivalent PSNR to x265. Our base layer was designed to support object detection, so it lacks the details needed to achieve high PSNR, and therefore needs to use a lot of bits to bring those details back in.

Fig. 13 and Table III show analogous results but with RGB-MS-SSIM as the frame quality metric. Learned codecs are known to perform better on MS-SSIM than on PSNR and, indeed, this is seen in Fig. 13 and Table III. Specifically, although VVenC still comes out as the best codec on BD-Rate-SSIM, the gap between it and our Enh (the second-best method) is now less than 1%. DCVC-TCM (the third-best method) also comes to within a few percentage points of VVenC. All other codecs perform comparatively better in Table III than in Table II. It is interesting to note that our Base method records the highest jump in performance between Table II and Table III. This suggests that object-relevant information, which is preserved in our base layer, is also favorable to quality metrics such as MS-SSIM.

Fig. 15 shows a patch from a sample frame from Race-Horses (HEVC Class C) reconstructed by various codecs at a similar bitrate: 0.42–0.44 bpp for all codecs, except our Enh at 0.37 bpp. As seen from these examples, learned codecs tend to suppress some details, especially in the grass in the background; among the learned codecs, LCCM-VC and the proposed one seem to have recovered most of these details. Fig. 16 shows visual comparisons of base and enhancement-





Fig. 16. Three examples of the visual quality of the base frame and the corresponding enhancement-layer reconstructed frame. Top row: a frame from RaceHorses (HEVC Class D, Base Rate=0.13, Enhancement Rate=0.05); Middle row: a frame from BasketballPass (HEVC Class D, Base Rate=0.07, Enhancement Rate=0.06); Bottom row: a frame from the TVD dataset (Base Rate=0.16, Enhancement Rate=0.08).

layer (reconstructed) frames produced by our codec. It is evident that base frames lack detail, but they preserve enough detail needed to identify objects, which is what the base layer is designed for.

### E. Break-Even Analysis

In the preceding sections, we provided experimental results for the machine task (object detection) and human viewing separately. We saw that the proposed scalable codec performs better than the alternatives on the machine task (Table I) while VVenC is the best-performing codec on frame reconstruction for human viewing (Tables II and III).

So, which codec is better – VVenC or the proposed one? That depends on how frequently one expects human viewing will be required in a particular application: whenever human viewing is needed, VVenC is better, but when the system performs the machine task only, the proposed codec is better. To enable numerical comparison of codecs in such a scenario, we adopt *break-even analysis* from [20]. The gist of break-even analysis is as follows. From Table I, the proposed codec is, on average, 16.8% (= 53.2% – 36.4%) more efficient than VVenC when the machine task is used. In other words, it uses 0.832 of the bits used by VVenC in this case. Meanwhile, from Table II, the proposed codec in the Enh regime is, on average, 23.9% (= 46.2% – 22.3%) less efficient than VVenC (it uses 1.239 of the VVenC bits) on frame reconstruction for human viewing, when frame quality is measured by RGB-PSNR. Let  $\phi \in [0, 1]$  be the fraction of time that input frame reconstruction is needed for human viewing. The amount of bits used by our system will be less than or equal to that used by VVenC if

$$(1 - \phi) \cdot 0.832 + \phi \cdot 1.239 \leq 1. \quad (24)$$

Solving for  $\phi$  that achieves equality in (24), we obtain the break-even point of  $\phi = 0.41$ . That is to say, if input reconstruction for human viewing is needed less than 41% of the time, our system will provide overall bit savings over VVenC. However, if RGB-MS-SSIM is used as the frame quality metric, we obtain  $\phi = 0.97$ . Using this analysis, the proposed method in the Enh regime always outperforms ( $\phi = 1$ ) the other codecs in this study, meaning that it provides bit savings regardless of the fraction of time used for human viewing. For completeness, Table IV also shows the break-even points of Base+Enh against VVenC. Although Base+Enh results are less favorable to our method and less realistic in a practical setting, as discussed earlier, even in this case our method provides gains over VVenC when human viewing is needed less than 27% of the time.

But how often is human viewing needed in these kinds of applications - traffic monitoring, surveillance, etc.? We do not have a precise answer to this question. One reference point could be a report published in 2015 [42], suggesting that less than 1% of all surveillance video is watched live. Given the proliferation of surveillance technology and likely much slower increase (if any) of human viewers of surveillance video, the percentage is almost certainly lower now. Although “human viewing” in our system is not the same as “live viewing,” the figure of 1% ( $\phi = 0.01$ ) can serve as a ballpark estimate, and we see in Table IV that the break-even points of our system are many-fold higher than that. In other words, our system could comfortably provide gains over VVenC in a practical surveillance scenario.

## V. CONCLUSION

In this manuscript, we provided a theoretical justification for conditional lossy coding, a technique whose rate-distortion

bounds are better than those of the commonly-used residual coding. We then presented the first end-to-end learned scalable video codec that employs conditional coding and is capable of efficiently supporting both human and machine vision. Specifically, object detection is supported by the codec's base layer, while input reconstruction for human viewing is supported by both the base and enhancement layer. We tested the proposed codec on the video object detection datasets used in MPEG-VCM, and compared it against recent learned and conventional video codecs. The results show that the proposed codec outperforms existing video codecs on the base task (object detection) while providing comparable performance to the best codecs on input frame reconstruction. We also performed break-even analysis against VVenC, the best-performing codec on input frame reconstruction, which showed that in a practical scenario, our codec is able to provide bit savings against VVenC if human viewing is needed less than 27% of the time.

## REFERENCES

- [1] L. Duan, J. Liu, W. Yang, T. Huang, and W. Gao, "Video coding for machines: A paradigm of collaborative compression and intelligent analytics," *IEEE Trans. Image Process.*, vol. 29, p. 8680–8695, 2020.
- [2] MPEG-CDVS, "Compact descriptors for visual search." ISO/IEC JTC 1 15938-13, 2015.
- [3] MPEG-CDVA, "Compact descriptors for video analysis." ISO/IEC JTC 1 15938-15, 2019.
- [4] G. J. Sullivan, J. R. Ohm, W. J. Han, and T. Wiegand, "Overview of the high efficiency video coding (HEVC) standard," *IEEE Trans. Circuits and Systems for Video Technology*, vol. 22, no. 12, 2012.
- [5] B. Bross, Y. K. Wang, Y. Ye, S. Liu, J. Chen, G. J. Sullivan, and J. R. Ohm, "Overview of the versatile video coding (VVC) standard and its applications," *IEEE Trans. Circuits and Systems for Video Technology*, vol. 31, no. 10, 2021.
- [6] J. Ballé, D. Minnen, S. Singh, S. J. Hwang, and N. Johnston, "Variational image compression with a scale hyperprior," in *Intl. Conf. on Learning Representations (ICLR)*, 2018, pp. 1–23.
- [7] D. Minnen, J. Ballé, and G. D. Toderici, "Joint autoregressive and hierarchical priors for learned image compression," in *Advances in Neural Information Processing Systems*, vol. 31, 2018.
- [8] Z. Cheng, H. Sun, M. Takeuchi, and J. Katto, "Learned image compression with discretized gaussian mixture likelihoods and attention modules," in *Proc. IEEE/CVF CVPR*, 2020.
- [9] J. Li, B. Li, and Y. Lu, "Deep contextual video compression," in *Advances in Neural Information Processing Systems*, 2021.
- [10] Y. H. Ho, C. P. Chang, P. Y. Chen, A. Gnutti, and W. H. Peng, "CANFVC: Conditional augmented normalizing flows for video compression," in *Proc. ECCV*, 2022.
- [11] Y. H. Ho, C. C. Chan, W. H. Peng, H. M. Hang, and M. Domanski, "ANFIC: Image compression using augmented normalizing flows," *IEEE Open Journal of Circuits and Systems*, vol. 2, pp. 613–626, 2021.
- [12] T. Ladune, P. Philippe, W. Hamidouche, L. Zhang, and O. Deforges, "Conditional coding for flexible learned video compression," in *Neural Compression From Information Theory to Applications-Workshop@ICLR 2021*, 2021.
- [13] E. Agustsson, D. Minnen, N. Johnston, B. J., H. S. J., and G. Toderici, "Scale-space flow for end-to-end optimized video compression," in *Proc. IEEE/CVF CVPR*, 2020, pp. 8503–8512.
- [14] X. Sheng, J. Li, B. Li, L. Li, D. Liu, and Y. Lu, "Temporal context mining for learned video compression," *IEEE Trans. Multimedia*, 2022.
- [15] W. Zhang, T. Yao, S. Zhu, and A. E. Saddik, "Deep learning-based multimedia analytics: a review," *ACM TOMCCAP*, vol. 15, 2019.
- [16] M. Rafie, L. Yu, Y. Zhang, and S. Liu, "[VCM] call for evidence for video coding for machines." ISO/IEC JTC 1/SC 29/WG 2, m55605, Oct. 2020.
- [17] Y. Hu, S. Yang, W. Yang, L.-Y. Duan, and J. Liu, "Towards coding for human and machine vision: A scalable image coding approach," in *Proc. IEEE ICME*, 2020.
- [18] K. Liu, D. Liu, L. Li, N. Yan, and H. Li, "Semantics-to-signal scalable image compression with learned revertible representations," *Int. J. Comput. Vis.*, p. 1–17, Jun. 2021.
- [19] H. Choi and I. V. Bajić, "Scalable image coding for humans and machines," *IEEE Trans. Image Process.*, vol. 31, p. 2739–2754, 2022.
- [20] —, "Scalable video coding for humans and machines," in *IEEE Int. Workshop on Multimedia Signal Process. (MMSP)*, Sep. 2022.
- [21] —, "Latent-space scalability for multi-task collaborative intelligence," in *Proc. IEEE ICIP'21*, Sep. 2021, p. 3562–3566.
- [22] T. M. Cover and J. A. Thomas, *Elements of Information Theory*, 2nd ed. Wiley, 2006.
- [23] G. Wang, C. Wu, X. Zhang, Z. Liu, and C. Shen, "YOLOv5: An effective single-stage object detector," in *IEEE/CVF CVPR*, 2021, pp. 14 138–14 147.
- [24] H. Hadizadeh and I. V. Bajić, "LCCM-VC: Learned conditional coding modes for video coding," in *IEEE ICASSP Workshops*, 2023, arXiv:2210.15883.
- [25] J. Redmon and A. Farhadi, "YOLOv3: An incremental improvement," *arXiv preprint arXiv:1804.02767*, Apr. 2018.
- [26] Y. Foroutan, A. Harell, A. de Andrade, and I. V. Bajić, "Base layer efficiency in scalable human-machine coding," *arXiv preprint arXiv:2307.02430*, 2023.
- [27] D. Sun, X. Yang, M. Liu, and J. Kautz, "PWC-Net: CNNs for optical flow using pyramid, warping, and cost volume," in *Proc. IEEE/CVF CVPR*, 2018, p. 8934–8943.
- [28] A. Harell, A. De Andrade, and I. V. Bajić, "Rate-distortion in image coding for machines," in *Proc. Picture Coding Symposium (PCS)*, 2022, pp. 199–203.
- [29] A. Harell, Y. Foroutan, N. Ahuja, P. Datta, B. Kanzariya, V. S. Somayaulu, O. Tickoo, A. de Andrade, and I. V. Bajić, "Rate-distortion theory in coding for machines and its application," *arXiv preprint arXiv:2305.17295*, 2023.
- [30] T. Xue, B. Chen, J. Wu, D. Wei, and W. Freeman, "Video enhancement with task-oriented flow," *Int. J. Computer Vision*, vol. 127, no. 8, pp. 1106–1125, 2019.
- [31] D. P. Kingma and J. Ba, "Adam: A method for stochastic optimization," in *International Conference for Learning Representations*, 2015.
- [32] G. Lu, C. Cai, X. Zhang, L. Chen, W. Ouyang, D. Xu, and Z. Gao, "Content adaptive and error propagation aware deep video compression," in *Proc. ECCV*, 2020, pp. 456–472.
- [33] Ultralytics, "The PyTorch implementation of YOLOv5," [https://pytorch.org/hub/ultralytics\\_yolov5/](https://pytorch.org/hub/ultralytics_yolov5/), 2022-12-01.
- [34] H. Choi, E. Hosseini, S. R. Alvar, R. A. Cohen, and I. V. Bajić, "A dataset of labelled objects on raw video sequences," *Data in Brief*, vol. 34, p. 106701, 2021.
- [35] X. Xu, S. Liu, and Z. Li, "Tencent video dataset (TVD): A video dataset for learning-based visual data compression and analysis," *arXiv preprint arXiv: 2105.05961*, 2021.
- [36] x265, "An open-source HEVC encoder," <https://x265.readthedocs.io/en/master/>, 2022-03-10.
- [37] A. Wiecekowski, J. Brandenburg, T. Hinz, C. Bartnik, V. George, G. Hege, C. Helmrich, A. Henkel, C. Lehmann, C. Stoffers, I. Zupancic, B. Bross, and D. Marpe, "VVenC: An open and optimized VVC encoder implementation," in *Proc. IEEE Int. Conf. on Multimedia Expo Workshops (ICMEW)*, 2021, pp. 1–2.
- [38] J. Lin, D. Liu, H. Li, and F. Wu, "M-LVC: multiple frames prediction for learned video compression," in *Proc. IEEE/CVF CVPR*, 2020, p. 3546–3554.
- [39] Z. Wang, E. Simoncelli, and A. Bovik, "Multiscale structural similarity for image quality assessment," in *Proc. Asilomar Conf. Signals, Systems, and Computers*, vol. 2, 2003, pp. 1398–1402.
- [40] G. Bjøntegaard, "Calculation of average PSNR differences between RD-curves," Apr. 2001, vCEG-M33.
- [41] M. Rafie, Y. Zhang, and S. Liu, "Evaluation framework for video coding for machines." ISO/IEC JTC 1/SC 29/WG 2, N41, Jan. 2021.
- [42] J. Honovich, "Live video monitoring usage statistics," IPVM Report, <https://ipvm.com/reports/live-video-monitoring-usage-statistics>, 2015-08-18.